DOI: 10.1002/anie.200604206

Microfabrication

Fabrication of Monodisperse Gel Shells and Functional Microgels in Microfluidic Devices**

*Jin-Woong Kim, Andrew S. Utada, Alberto Fernández-Nieves, Zhibing Hu, and David A. Weitz**

Microgels are colloidal gel particles that consist of chemically cross-linked three-dimensional polymer networks; these networks are able to dramatically shrink or swell by expelling or absorbing large amounts of water in response to external stimuli.[1,2] The large change in size can be achieved, for example, by modifying the pH, temperature, or ionic strength of the medium, or by applying electric or magnetic fields; it is this response that makes microgels desirable for applications in drug delivery,[3,4] biosensing,[5] diagnostics,[6,7] bioseparations,[8] and optical devices.[9,10] To further expand their range of applicability, there have been efforts to generate microgels that have been complexed with preformed functionalized materials that impart additional desirable properties to the microgel.[11–14] These preformed materials range from molecules to microparticles and are typically complexed with the gel matrix through specific interactions. The resulting complexed microgels usually show a drastic decrease in their physical response to external stimuli compared to that of the original cross-linked polymer networks;[15–17] this is an undesirable side effect since the microgel performance for a given application is based on its sensitivity to external stimuli. In addition to functionality, the size distribution of a population of microgels is important; it is critical to provide a homogeneous distribution of microgels applying formulations[18] and in controlling the release kinetics of encapsulates or adsorbents.[19] From the standpoint of performance and applicability, there is a need for methods to generate monodisperse microgels that maintain high sensitivity to external stimuli irrespective of the materials that are incorporated to add complementary functions.

Here, we describe a flexible and straightforward method for generating monodisperse suspensions of new microgel-based materials using a capillary microfluidic technique.[20] This technique enabled us to generate and precisely control the size of the microgel-based particles[21–23] without sacrificing the physical response of the resulting microgels. We generated two novel microgel structures: a spherical microgel shell and spherical microgel particles that retain their full sensitivity to external stimuli after being physically complexed with preformed colloidal particles. The overall size and thickness of the microgel shells can be tuned with temperature. We generated the spherical microgel particles in a single step, which allows us to freely incorporate functional materials into the polymer network. We used quantum dots, magnetic nanoparticles, and polymer microparticles as examples of the materials that can be added to provide specific chemical, physical, or mechanical properties to the original microgels.

To generate the microgel particles, we constructed a capillary-based microfluidic device that generated pre-microgel drops, which were then polymerized in situ with a redox reaction.[24] The capillary microfluidic device was made of three separate capillary tubes. The two internal cylindrical tubes served as injection and collection tubes and were coaxially aligned, as shown in the inset in Figure 1 A. These tapered tubes were made by axially heating and pulling cylindrical capillaries. In the region near both tips, the outer fluid focuses both the middle and inner fluids through the collection tube to form a fluid thread that then breaks into drops as a result of hydrodynamic instabilities, as shown in Figure 1 A. We typically used silicon oil with viscosity $\eta_{OF} = 125$ mPa s as the outer, or continuous-phase liquid. The middle fluid was an aqueous monomer solution that contained *N*-isopropylacrylamide (NIPAm, 15.5 % w/v), a cross-linker (*N*,*N*′-methylenebisacrylamide, BIS, 1.5 % w/v), a reaction accelerator (*N*,*N*,*N*′,*N*′-tetramethylethylenediamine, 2 vol %), and two co-monomers [2-(methacryloyloxy) ethyl trimethyl ammonium chloride (METAC, 2 vol %) and allylamine (1 vol %)]. METAC was added to increase the coil-to-globule transition temperature of poly(NIPAm), thereby facilitating homogeneous polymerization at room temperature. The allylamine adds amine groups to the network, which can subsequently be labeled with dyes after the formation of the microgel particles. The chemical formula

[*] Dr. J. W. Kim, A. S. Utada, Dr. A. Fernández-Nieves, Prof. D. A. Weitz
DEAS and Department of Physics
Harvard University
Cambridge, MA 02138 (USA)
Fax: (+1) 617-495-2875
E-mail: weitz@deas.harvard.edu
Dr. J. W. Kim
Amore-Pacific R&D Center
314-1, Bora-dong, Giheung-gu, Yongin-si
Gyeonggi-Do, 446-729 (Korea)
Dr. A. Fernández-Nieves
Interdisciplinary Network of Emerging Science and Technology (INEST) Group
Research Center, Phillip Morris USA
Richmond, VA 23298 (USA)
Prof. Z. Hu
Department of Physics, University of North Texas
Denton, TX 76203 (USA)

[**] This work was supported by the Postdoctoral Fellowship Program of Korea Research Foundation (KRF) and Amore-Pacific Co. (Korea), and by the NSF (DMR-0602684 (D.A.W.) and DMR-0507208 (Z.H.)) and the Harvard MRSEC (DMR-0213805). A.F.-N. is grateful to the Ministerio de Ciencia y Tecnologia (MAT2004-03581) and to the University of Almeria (leave of absence). INEST Group is sponsored by PMUSA.

Supporting information for this article is available on the WWW under http://www.angewandte.org or from the author.

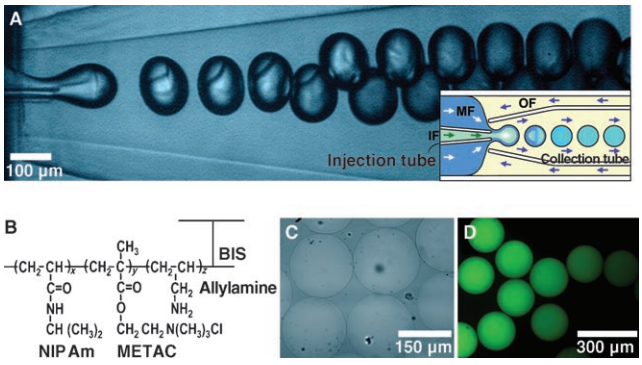

Figure 1. A) Drop formation of pre-microgel drops in a capillary microfluidic device. The inset shows the device geometry. The inner diameter of the end of the injection tube through which inner fluid was injected is approximately 20 μm. The inner diameter of the collection tube is about 200 μm. The outer fluid (OF) is silicon oil (DC #550, density = 1.06 g mL^{-1}). The middle fluid (MF) is an aqueous solution containing NIPAm, BIS, METAC, allylamine, and *N*,*N*,*N*′,*N*′-tetramethyethylenediamine. The inner fluid (IF) is an APS solution. The density of water phase is matched to 1.05 g mL^{-1} by mixing glycerol (10 vol%) and deuterium oxide (22 vol%). B) The molecular structure of poly(NIPAm) microgel network. C) A bright-field microscope image of poly(NIPAm) microgels in water. D) A fluorescence image of fluorescein isothiocyanate (FITC)-labeled poly(NIPAm) microgels.

for the gel network is shown in Figure 1 B. The inner fluid was an aqueous solution containing the initiator (ammonium persulfate, APS, 3% w/v). We matched the densities of the aqueous middle and inner fluids to approximately 1.05 g mL^{-1} to ensure good mixing of the two liquids inside the drops and prevent creaming or sedimentation of suspending materials. After the pre-microgel drops had formed, uniform mixing of the middle and inner fluids required approximately 90 ms, whereupon the cross-liking reaction was initiated; complete cross-linking of the drops required about 10 s at room temperature. Owing to the speed of the polymerization, surfactants were not needed to prevent coalescence of the pre-microgel drops as they flowed down the collection tube. By tuning the flow rates of the three fluid streams, we were able to produce microgel particles at rates from 10^2 to 10^3 Hz, which we measured using high-speed imaging. After we collected the microgel particles, they were washed repeatedly with large amounts of isopropyl alcohol to remove the silicon oil, and then transferred to deionized water. Since the microgels were nearly transparent in water, we reacted fluorescein isocyanocyanate with the amine groups in the gel network to better visualize them as well as to explore the homogenity of the network itself. Bright-field and fluorescence images of the resultant microgels are shown in Figure 1 C, D. The uniform fluorescence intensity within the particles confirmed that they were homogeneous.

To better control the size and composition of microgels, we examined the physical mechanism of the pre-microgel drop formation. The pre-microgel drops formed within the collection tube at approximately one tube diameter downstream from the entrance.[20,25–27] When drops formed close to the entrance of the tube, the drop size was controlled by the ratio of the flow rates of the combined inner and middle fluids to the outer fluid, which is given by Equation (1), where Q_{sum} is the sum of the of inner and middle fluid flow rates, R_{thread} is

$$Q_{sum}/Q_{OF} = \pi R_{thread}^2/(\pi R_{orifice}^2 - \pi R_{thread}^2) \quad (1)$$

the radius of the fluid thread that breaks into drops, and $R_{orifice}$ is the radius of the collection tube where the drops are formed. This equation is valid for plug-flow (Figure 2 B), which is a reasonable assumption given the proximity of drop formation to the entrance of the collection tube. The experimentally measured diameters of different threads and the corresponding drops that pinch from these threads are shown as the open and closed symbols, respectively, in Figure 2. By solving for $R_{thread}/R_{orifice}$ in Equation (1) and plotting it as a function of Q_{sum}/Q_{OF}, we can quantitatively predict the experimentally measured values, as shown by the dashed line in Figure 2. When a fluid thread breaks, the diameter of the resulting drop is proportional to the diameter

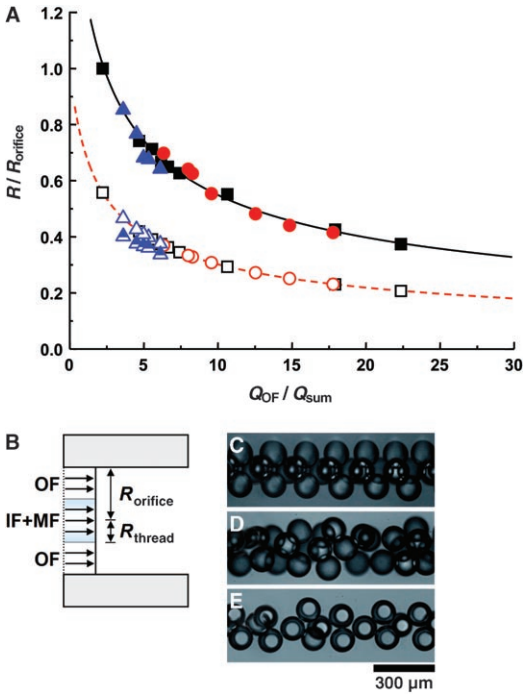

Figure 2. A) Dependence of thread radius R_{thread} and drop radius R_{drop} on the scaled flow rate Q_{OF}/Q_{sum}. The open symbols represent the R_{thread} for different pre-microgel liquids: the pre-microgel liquid only (□), the same pre-microgel liquid containing 1-μm polystyrene (PS) particles (≈0.22 vol%, ○) and double emulsions consisting of a single silicon drop surrounded by a pre-microgel liquid shell ($3Q_{IF} = Q_{MF}$, △). The dashed line represents the predicted R_{thread}. R_{drop} values are represented with solid identical symbols. Half-filled triangles correspond to the radius of the internal silicone droplets of the double emulsions employed to generate the microgel shells. The solid line represents the predicted R_{drop}. B) The flat velocity profile of the flow as it enters the capillary tube. C) Pre-microgel droplets flowing through the collection tube. D) Pre-microgel droplets containing 1 μm PS particles. E) Pre-microgel droplets, each containing a single internal silicon oil droplet. The flux change caused by incorporating colloid particles into the corresponding fluids is negligible. The ratio of viscosities, $\eta_{MF}/\eta_{OF} \approx 0.08$. The radii of pre-microgel drops showed that $R_{drop} = 1.82R_{thread}$, in agreement with what is expected theoretically.[20,28] Flow rates were controlled with stepper-motor-controlled syringe pumps (Harvard Apparatus).

of the thread as well as the viscosity ratio. For a viscosity ratio of $\eta_{MF}/\eta_{OF} \approx 0.1$, the drop diameter is approximately twice the diameter of the thread.[28] We neglected the decrease in viscosity due to the contribution of the inner liquid because its volume fraction in the drop is small. By multiplying the predicted thread diameter by a factor of two, we again saw very good agreement between the model and the data. These simple physical arguments highlight the versatility of this method in generating microgels of different sizes without losing monodispersity of the suspension (see Figure 2C–E); typical standard deviations in size are less than 2.5%.

An additional advantage of our microfluidic approach is that the different input streams remain separate up to the point of drop formation. Since the flow rates of the three fluids determine the size of the thread and ultimately, the drop size, we can incorporate virtually any materials that do not appreciably change the viscosities of the middle fluid into either the inner and middle fluids, and we can still predict R_{drop} accurately. By using these advantages, we have generated a novel spherical microgel shell that is suspended in water and has an aqueous core, as shown in Figure 3A. We generated this structure by initially using an oil as the inner fluid, which is immiscible with the aqueous middle fluid; these drops pinch-off to produce uniform double emulsions, where each aqueous pre-microgel drop contains a single oil droplet. In this case, the initiator is located in the middle fluid while the accelerator is dissolved in the inner oil. Upon forming the double-emulsion drops, the acclerator diffuses from the internal oil droplet into the surrounding aqueous monomer solution layer, initiating the polymerization. After collecting the microgel shell particles, we extracted the oil by washing with an excess of isopropyl alcohol and finally transferred the particles into deionized water. The overall diameter and thickness of these microgel shells can be tuned by changing the relative flow rates of the fluids during drop formation. Once these novel microgel shells were generated, we probed their thermosensitivity by measuring changes in the inner and outer radii as a function of temperature, as shown in Figure 3B. Both radii decrease with increasing temperature and showed no signs of hysteresis after repeated cooling and heating of the sample; however, while the core reached a minimum volume at about 50°C, the overall volume of the shell still decreased. This is seen more easily by plotting the volume of the core scaled by the overall particle volume as shown in Figure 3C; this ratio sharply increases at approximately 50°C, indicating that above this temperature the shell itself shrinks while the core volume remains unchanged. We believe that the microgel shell becomes more hydrophobic and denser as the temperature increases, which reduces the permeability to water molecules and ultimately limits the degree to which the volume of the core can change.

The versatility of this microfluidic approach also enables the synthesis of microgel particles that contain micro- or nanoparticles. We demonstrated the production of monodisperse poly(NIPAm) microgels containing polystyrene microparticles, quantum dots, and magnetic nanoparticles. Images of these hybridized microgels are shown in Figure 4A–C. The robustness of this approach allowed the engineering of microgels that encapsulate or immobilize colloidal materials within their network, thereby physically locking in these particles and confering unique properties to the original microgels. Unlike other methods that yield microgels with less sensitivity to stimuli, these complex microgels exhibit the same physical response to temperature changes as the original microgels, irrespective of the material incorporated into the gel matrix (Figure 4D). We attribute this to the fact that the added materials are physically trapped within the gel network rather than being chemically linked through some specific interactions. Moreover, the surfaces of the colloidal particles were all chemically treated with either polyethylene glycol chains or amine groups to prevent interactions. As expected for any poly(NIPAm) gel, the volume decreases with increasing temperature; however, the transition temperature, which is about 50°C, is higher than that of most common poly(NIPAm) microgels, which are typically about 32°C. This change is due to the presence of charged co-monomers in the polymer network that contribute to the total osmotic pressure, ultimately shifting the system's transition to higher temperatures. We also note that the colloidal particles are unable to escape from the microgels even at the lower temperatures where the microgels are swollen because the colloids are larger than the mesh size of the gel network. The mesh size of the network is determined by the concentration of cross-linker in our microgels ($\approx 7.5\%$ w/v).

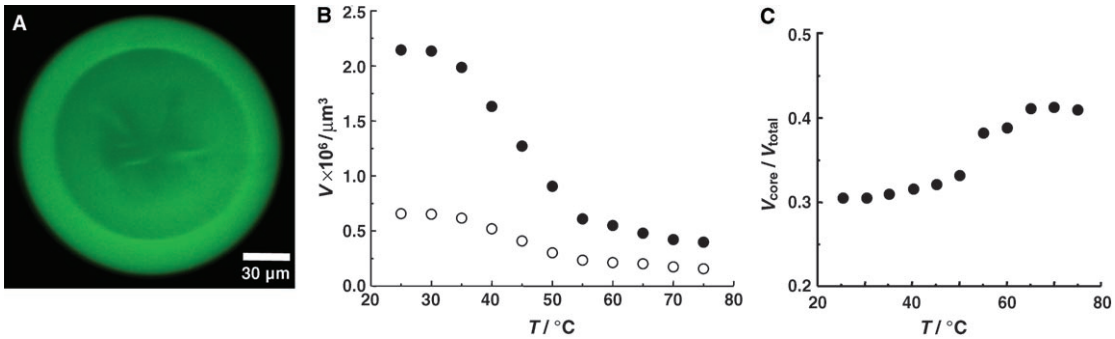

Figure 3. A) A fluorescence microscope image of an FITC-labeled microgel shell that is prepared from a pre-microgel double emulsion that contained a single silicon oil droplet. The concentrations of the colloidal particles and fluorescent dyes are determined against pre-microgel volumes before the microfluidic process. B) Volume changes of the overall core–shell poly(NIPAm) microgel (●) and its internal void (○). C) Volume of the internal void scaled by the volume of the whole microgel as a function of temperature. The core–shell microgels were prepared under the following flow conditions: $Q_{IF} = 100\ \mu L\,h^{-1}$, $Q_{MF} = 300\ \mu L\,h^{-1}$, and $Q_{OF} = 2000\ \mu L\,h^{-1}$. All swelling measurements were carried out in water.

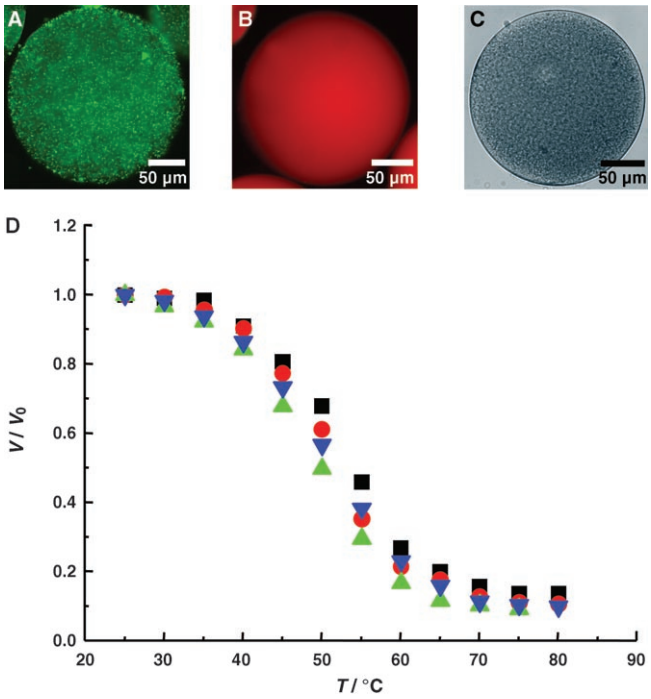

Figure 4. A) A fluorescence microscope image of a microgel containing 1-μm diameter fluorescent PS particles at approximately 0.22 vol%. These particles are covered with NH_2 groups. B) A fluorescence microscope image containing 19-nm quantum dots at 10 vol% of 2 μM. These quantum dots have a PEG-covered surface. C) A bright-field microscope image of a microgel-containing 10-nm magnetic particles at approximately 0.25 vol%. These particles are stabilized with a cationic surfactant. D) Volume transitions of poly(NIPAm) microgels (■) and poly(NIPAm) microgels that contain quantum dots (●), magnetic nanoparticles (▲), and PS microparticles (▼). Microgels were prepared under the following flow conditions: $Q_{IF} = 200\ \mu L\,h^{-1}$, $Q_{MF} = 200\ \mu L\,h^{-1}$, and $Q_{OF} = 2000\ \mu L\,h^{-1}$. All swelling measurements were carried out in water.

In conclusion, we have shown that microfluidics allows fabrication of monodisperse temperature-sensitive microgels, in which a variety of additional materials can be incorporated naturally into the gel network or core-shell morphologies generated. Furthermore, this approach also allows control of the particle size in the range 10–1000 μm without the need to sacrifice the monodispersity of the sample. The core-shell microgels show a unique volume transition behavior in response to temperature changes. This particular behavior is of great importance for potential delivery applications, allowing unstable biomaterials, such as drugs and biomolecules, to be stored in the stable water-filled core of these microgel shells and be delivered, controllably, utilizing the unique physical behavior of their temperature response. These characteristics highlight the robustness and versatility of our microfluidic approach in generating more complex microgel particles, which could be used to develop novel biomaterials for applications in drug delivery, artificial muscles, and cancer therapy.

Received: October 13, 2006
Published online: January 30, 2007

Keywords: colloids · gels · microfluidics · polymers

[1] B. R. Saunders, B. Vincent, *Adv. Colloid Interface Sci.* **1999**, *80*, 1–25; V. Nerapusri, J. L. Keddie, B. Vincent, I. A. Bushnak, *Langmuir* **2006**, *22*, 5036–5041; M. Bradley, J. Ramos, B. Vincent, *Langmuir* **2005**, *21*, 1209–1215.
[2] Y. Qiu, K. Park, *Adv. Drug Delivery Rev.* **2001**, *53*, 321–339.
[3] N. Murthy, M. Xu, S. Schuck, J. Kunisawa, N. Shastri, J. M. Frechet, *Proc. Natl. Acad. Sci. USA* **2003**, *100*, 4995–5000.
[4] R. Langer, N. A. Peppas, *AIChE J.* **2003**, *49*, 2990–3006.
[5] J. H. Holtz, S. A. Asher, *Nature* **1997**, *389*, 829–832.
[6] T. Miyata, M. Jige, T. Nakaminami, T. Uragami, *Proc. Natl. Acad. Sci. USA* **2006**, *103*, 1190–1193.
[7] K. G. Olsen, D. J. Ross, M. J. Tarlov, *Anal. Chem.* **2002**, *74*, 1436–1441.
[8] F. Arai, C. Ng, H. Maruyama, A. Ichikawa, H. El-Shimy, T. Fukuda, *Lab Chip* **2005**, 5, 1399–1403.
[9] Z. Hu, G. Huang, *Angew. Chem.* **2003**, *115*, 4947–4950; *Angew. Chem. Int. Ed.* **2003**, *42*, 4799–4802; Z. Hu, X. Lu, J. Gao, *Adv. Mater.* **2001**, *13*, 1708–1712.
[10] J. D. Debord, L. A. Lyon, *J. Phys. Chem. B* **2000**, *104*, 6327; J. D. Debord, S. Eustis, S. B. Debord, M. T. Lofye, L. A. Lyon, *Adv. Mater.* **2002**, *14*, 658.
[11] R. Langer, D. A. Tirrell, *Nature* **2004**, *428*, 487–492; D. G. Anderson, J. A. Burdick, R. Langer, *Science* **2004**, *305*, 1923–1924.
[12] R. Pelton, *Adv. Colloid Interface Sci.* **2000**, *85*, 1–33.
[13] S. Nayak, A. L. Lyon, *Angew. Chem.* **2004**, *116*, 6874–6877; *Angew. Chem. Int. Ed.* **2004**, *43*, 6706–6709.
[14] I. Berndt, J. S. Pederson, W. Richtering, *Angew. Chem.* **2006**, *118*, 1769–1773; *Angew. Chem. Int. Ed.* **2006**, *45*, 1737–1741.
[15] L. Rogach, D. Nagesha, J. W. Ostrander, M. Giersig, N. A. Kotov, *Chem. Mater.* **2000**, *12*, 2676–2685.
[16] J. Zhang, S. Xu, E. Kumacheva, *J. Am. Chem. Soc.* **2004**, *126*, 7908–7914.
[17] A. Pich, A. Karak, Y. Lu, A. K. Ghosh, H.-J. P. Adler, *Macromol. Rapid Commun.* **2006**, *27*, 344–350.
[18] K. Shiga, N. Muramatsu, T. Kondo, *J. Pharm. Pharmacol.* **1996**, *48*, 891–895; N. Muramatsu, K. Shiga, T. Kondo, *J. Microencapsulation* **1994**, *11*, 171–178.
[19] X.-C. Xiao, L.-Y. Chu, W.-M. Chen, S. Wang, R. Xie, *Langmuir* **2004**, *20*, 5247–5253.
[20] S. Utada, E. Lorenceau, D. R. Link, P. D. Kaplan, H. A. Stone, D. A. Weitz, *Science* **2005**, *308*, 537–541; D. R. Link, E. Grasland-Mongrain, A. Duri, F. Sarrazin, Z. Cheng, G. Cristobal, M. Marquez, D. A. Weitz, *Angew. Chem.* **2006**, *118*, 2618–2622; *Angew. Chem. Int. Ed.* **2006**, *45*, 2556–2560; E. Lorenceau, A. S. Utada, D. R. Link, G. Cristobal, M. Joanicot, D. A. Weitz, *Langmuir* **2005**, *21* 9183–9186.
[21] F. Ikkai, S. Iwamoto, E. Adachi, M. Nakajima, *Colloid Polym. Sci.* **2005**, *283*, 1149–1153; S. Sugiura, M. Nakajima, N. Kumazawa, S. Iwamoto, M. Seki, *J. Phys. Chem. B* **2002**, *106*, 9405–9409.
[22] B. G. De Geest, J. P. Urbanski, T. Thorsen, J. Demeester, S. C. De Smedt, *Langmuir* **2005**, *21*, 10275–10279.
[23] H. Zhang, E. Tumarkin, R. Peerani, Z. Nie, R. M. A. Sullan, G. C. Walker, E. Kumacheva, *J. Am. Chem. Soc.* **2006**, *128*, 12205–12210.
[24] E. Sato, T. Tanaka, *J. Chem. Phys.* **1988**, *89*, 1695–1703; Y. Hirose, T. Amiya, Y. Hirokawa, T. Tanaka, *Macromolecules* **1987**, *20*, 1342–1344.
[25] B. Ambravaneswaran, H. J. Subramani, S. D. Phillips, O. A. Basaran, *Phys. Rev. Lett.* **2004**, *93*, 034501–4.
[26] C. Clanet, J. C. Lasheras, *J. Fluid Mech.* **1999**, *383*, 307–326.
[27] W. M. Deen, *Analysis of Transport Phenomenon*, Oxford Press, Oxford, **1998**, p. 265.
[28] S. Tomotika, *Proc. R. Soc. London Ser. A* **1935**, *150*, 322–337.

